Nationaal Lucht- en Ruimtevaartlaboratorium

National Aerospace Laboratory NLR

Executive summary
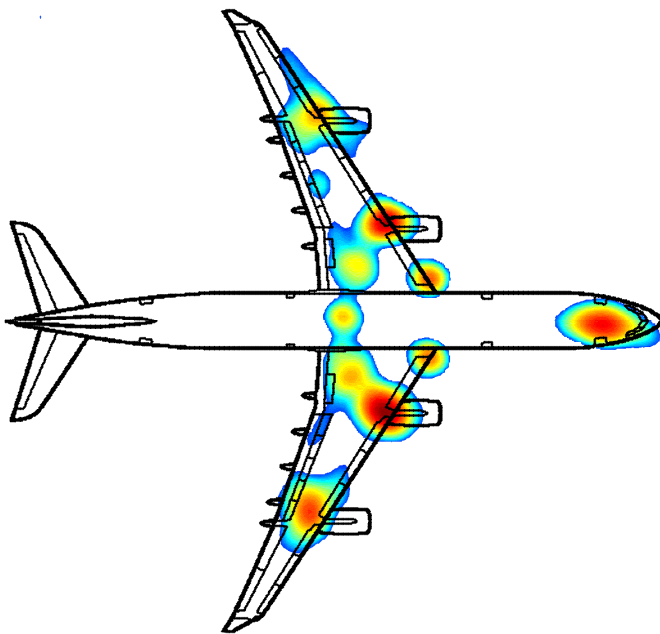
Phased array beamforming applied to wind tunnel and fly-over tests

Problem area
This paper discusses methods of acoustic source location for wind tunnel and fly-over measurements.

Description of work
An introduction is given of phased array beamforming techniques for locating acoustic sources. Starting from basic principles, the Conventional Beamforming technique is described. It is explained how this technique can be applied to wind tunnel measurements. Further, a number of advanced array processing techniques are discussed. One chapter is devoted to the array processing technique for the location of moving sources. This technique can be applied to rotating sources, for example on wind turbine blades, and to source location on aircraft flying over a microphone array.

Applicability
The methods described in this paper can be applied to wind tunnel and fly-over microphone array measurements.

This report is based on an invited lecture held at the II SAE Brasil International Noise and Vibration Congress, Florianópolis, SC, Brasil, 17-19 October 2010.

Phased array beamforming applied to wind tunnel and fly-over tests

P. Sijtsma

Summary

An introduction is given of phased array beamforming techniques for locating acoustic sources. Starting from basic principles, the Conventional Beamforming technique is described. It is explained how this technique can be applied to wind tunnel measurements. Further, a number of advanced array processing techniques are discussed. One chapter is devoted to the array processing technique for the location of moving sources. This technique can be applied to rotating sources, for example on wind turbine blades, and to source location on aircraft flying over a microphone array.

Contents

4

Nomenclature

<u>Symbols</u>

A	source auto-power
$A_{1,2}$	source cross-power
A_{max}	peak level of A_h; or maximum array output, see Eq. (78)
A_{mod}	modified source auto-power, see Eq. (79)
$A_{s,h}$	source auto-power estimate of simulated point source
$A_{s,max}$	peak level of $A_{s,h}$
$\tilde{A}_h$	see Eq. (69)
$\tilde{A}_{s,h}$	see Eq. (70)
a	complex pressure amplitude at source
B	constant: $B = f \times R(f)$, see Eq. (57)
$\mathbf{C}$	cross-power matrix
$\mathbf{C}_{max}$	cross-power matrix induced by source in $\vec{\xi}_{max}$
C_{mn}	microphone cross-power
C_{nn}	microphone auto-power
c	speed of sound
d_{mn}	see Eq. (51)
D	array diameter
$\mathbf{E}$	diagonal matrix with eigenvalues of $\mathbf{C}$
Erf	Error function
$\vec{e}_x$	unit vector in x-direction
F	transfer function from moving source in $\vec{\xi}(t)$ to receiver in $\vec{x}$
F_n	transfer function from $\vec{\xi}(t)$ to n-th microphone (cf. Eqs. (104) and (105))
f	frequency
f_{max}	maximum frequency
f_{sam}	sample frequency
G	Green's function
G_{mn}	cross-spectral density function
g	steering function
$\mathbf{g}$	steering vector
$\mathbf{g}_l$	steering vector corresponding with source in $\vec{\xi}_l$
$\mathbf{g}_{max}$	transfer vector corresponding with peak source location $\vec{\xi}_{max}$
$\mathbf{H}$	matrix containing the diagonal elements of $\mathbf{hh}^*$
H	number of grid points
$\mathbf{h}$	approximation for $\mathbf{g}_{max}$, see Eq. (84)

h	grid index
i	imaginary unit
j	frequency index
J	cost function
J_0	zero-th order Bessel function of the first kind
K	number of samples during one time period (block size)
k	sample index
L	number of eigenvalues
M	Mach number of uniform flow
$\vec{M}$	Mach number vector of uniform flow
m	microphone index
N	number of microphones
n	microphone index
P	integrated source power
P_s	source power of simulated monopole
$\mathbf{p}$	pressure vector
$p(\vec{x})$	complex acoustic pressure amplitude
p_n	complex pressure amplitude at n-th microphone
$\mathbf{Q}$	matrix with eigenvectors of $\mathbf{C}$
q	see Eq. (3)
$R(f)$	aperture radius
$R_{mn}(t)$	cross-correlation function
r_n	see Eq. (56)
S	set of pairs (m,n) for which C_{mn} is not discarded
T	time period ($T = K\Delta t$)
t	time
t_1	see Eq. (94)
t_n	reception time at n-th microphone
$\vec{U}$	uniform flow speed
u_k	weight factor for FFT window
v_n	weight factor for spatial window
W	aperture smoothing function
$\mathbf{w}$	weight vector for beamforming
$\mathbf{w}_{\max}$	steering vector corresponding with peak source location $\vec{\xi}_{\max}$
$\vec{x}$	Cartesian position vector
$\vec{x}_1$	see Eq. (94)
$\vec{x}_n$	location of n-th microphone

x_n	x-component of location of n-th microphone
Y	distance between source and array
y_n	y-component of location of n-th microphone
Z	dynamic range for source power integration
z_n	z-component of location of n-th microphone

Greek

$\vec{\alpha}$	wave number vector
$\alpha_{\min}$	minimum value for $\|\vec{\alpha}\|$
$\alpha_{\max}$	maximum value for $\|\vec{\alpha}\|$
α_x	x-component of $\vec{\alpha}$
α_y	y-component of $\vec{\alpha}$
β	see Eq. (30)
γ	auxiliary function in Eq. (100)
Δt	sample interval ($\Delta t = 1/f_{\text{sam}}$)
Δt_e	emission time delay
δ	Dirac delta function
$\varepsilon_n(t)$	noise on n-th microphone
φ	loop gain used in CLEAN algorithm
$\chi(\vec{x},t)$	acoustic pressure field
$\chi_n(t)$	fluctuating pressure measured by n-th microphone
$\chi_{n,k}$	sampled acoustic pressure measured by n-th microphone
λ_n	weight factor for microphone density
μ_n	weight factor for effective aperture
ν	averaging index
$\sigma(t)$	emitted source signal
$\tilde{\sigma}(t)$	estimated source signal
τ	integration parameter (time)
τ_0	zero of auxiliary function γ, Eq. (100)
τ_e	emission time
$\vec{\xi}$	source location
$\vec{\xi}_{\max}$	peak source location
ζ	z-value of source location
Ω	sub-area of array

Operator

∇	Nabla operator: $\nabla = \left(\partial/\partial x, \partial/\partial y, \partial/\partial z \right)$

8

Superscript

$(\cdot)^*$ complex conjugate (transpose)

Subscript

$(\cdot)_a$ induced by acoustic pressure

$(\cdot)_j$ for j-th frequency

$(\cdot)_h$ for h-th grid point

$(\cdot)_k$ for k-th sample

$(\cdot)_l$ for l-th source

$(\cdot)_m$ for m-th microphone

$(\cdot)_n$ for n-th microphone

$(\cdot)_s$ corresponding to simulated point source

$(\cdot)_{sl}$ corresponding to shear layer

$(\cdot)_w$ induced by wind

$(\cdot)_\nu$ for ν-th FFT block; or after ν averages

Abbreviations

DNW   German-Dutch Wind Tunnels

FFT   Fast Fourier Transform

LST   Low-speed Wind Tunnel

LLF   Large Low-speed Facility

This page is intentionally left blank.

1 Introduction

Public opinion demands a quiet environment. Therefore, there is a continuous pressure to reduce noise from industry, cars, trains, aircraft, wind turbines, etc. In order to reduce noise, it is important to understand the noise generation process. Sometimes, noise sources are well known, and solutions are evident (e.g. insulation). In many cases, however, the noise origin is not obvious. Even the actual location of the (loudest) noise source may be unknown. Knowledge of the source location is, of course, the first step towards noise reduction.
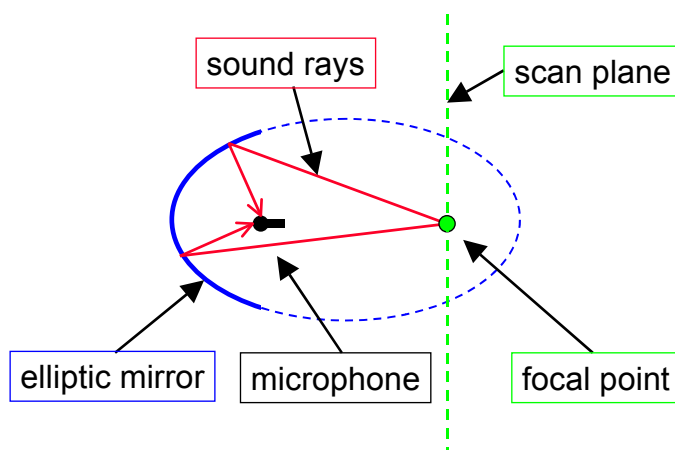
Figure 1 Principle of elliptic mirror

A possibility to locate acoustic sources is by means of an elliptic "acoustic" mirror (Refs. 1, 2). The concept of an acoustic mirror is based on the fact that acoustic rays emerging from one focal point of the ellipse converge to the other focal point (see Figure 1). A microphone is placed in the focal point close to the mirror, while the other focal point scans through a surface of possible noise sources. This scanning can be done by traversing the mirror or by moving the studied object. An example of a set-up with an acoustic mirror in the DNW-LLF wind tunnel is shown in Figure 2.

By scanning with acoustic mirrors, source locations can be found with high accuracy. Sources close to each other can be separated well. The range of frequencies to which acoustic mirrors can be applied is large. Furthermore, background noise is filtered out effectively. The main drawback of acoustic mirrors is the long time that is needed for measurements. The mirror (or the studied object) has to be moved for each scan point. Consequently, measurements with acoustic mirrors are expensive, especially in large wind tunnels.

Since the 1970's (Refs. 3, 4) developments are ongoing on the alternative for the acoustic mirror: the "acoustic array" or "microphone array". A microphone array is a set of microphones,

of which the signals are combined in such a way that sound from a specified focal point is amplified and sound from other directions is attenuated. This signal combination is done through appropriately delaying and summing the individual microphone signals. In the frequency-domain this boils down to applying microphone-dependent phase shifts. Thus, the microphone array is a special type of "phased array", also applied in seismology, astronomy and underwater acoustics (sonar). The advantage of microphone arrays compared to acoustic mirrors is that only short measurement time is needed, because the process of scanning through possible source locations is performed afterwards.

Figure 2 Set-up with acoustic mirror in DNW-LLF open jet

Until the mid 1990's, the microphone array could not outperform the acoustic mirror in spatial resolution, frequency range and signal/noise ratio. The main reason for this was the limited capacity of data-acquisition systems (data-loggers), so that the number of microphones had to be limited. Nowadays, however, the large capacity of computers and data acquisition systems enable the use of large numbers of microphones, long acquisition times and high sample frequencies (Ref. 5). Thus, the traditional drawbacks of microphone arrays compared to acoustic mirrors, namely lower resolution and lower signal/noise ratio, are vanishing. What remains is the great advantage of arrays, that is, the short time needed for measurements.

In addition, microphone arrays offer the opportunity to locate sources on moving objects. This application has been implemented on objects in steady, rectilinear motion, like trains passing by (Refs. 6, 7) and airplanes flying over (Refs. 8-10). The technique of de-Dopplerisation (Refs. 11, 12) was applied to recalculate, from the microphone signals, the source signals in the moving frame. In reference 13, it was shown that acoustic source location by a microphone

array is, in principle, possible on objects in any given subsonic motion. Besides, it was made clear that the presence of a uniform flow does not form a limitation. Therefore, source location measurements on arbitrarily moving objects in wind tunnels are feasible too. In reference 13, applications were shown to rotating sources like rotating whistles and broadband noise sources on wind turbine and helicopter blades.

The technique of locating sources using phased arrays is called "beamforming". Basically, it is an algorithm, applied to each scan point individually, which amplifies the sound from the scan point and attenuates the sound from other directions. The source is then identified as the scan point from which the beamforming algorithm yields maximum output. There are a large number of beamforming techniques available (Ref. 14), e.g. developed for Astronomy. Many of those, however, are not well applicable to acoustics. Here, we limit ourselves to those techniques that are able to cope with the specific difficulties of acoustic measurements, such as background noise, coherence loss, errors in the transfer model, and microphone calibration uncertainties.

This paper discusses microphone array measurements of aircraft and their components in wind tunnels, and by means of fly-over tests. It is well established that such measurements are able to quantify differences in sound source levels, e.g., as a result of model modifications. This can be done by processing the measurements with the commonly used Conventional Beamforming technique (Ref. 14). Extraction of absolute acoustic source levels is more difficult, but not impossible. Methods for obtaining the absolute levels depend on the test environment.
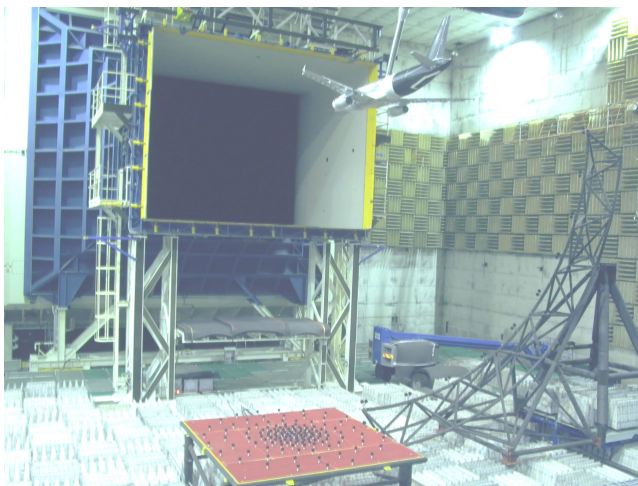
Figure 3 Set-up with microphone array in DNW-LLF open jet

In open jet wind tunnels, where the microphones are usually out-of-flow (see Figure 3), the main difficulty is the presence of the shear layer between the wind tunnel model and the microphone array. The shear layer causes loss of coherence between microphone signals (Ref. 15), and, as a result, the beamforming process underpredicts the source levels. In fact, the

predicted source levels become dependent on array size (Ref. 16). The Source Power Integration technique (Refs. 16) can be used to overcome this problem.

In closed test sections (see Figure 4), where the microphones are usually mounted flush in the wall, the main issue is boundary layer noise. Boundary layer noise is of hydrodynamic nature, and is due to turbulence in the boundary layer. Boundary layer noise levels are often much higher than the levels of the sound radiated from the wind tunnel model. This can severely affect the beamforming results. Fortunately, because boundary layer noise is incoherent from one microphone to the other, it will appear only in the auto-spectra, and not in the cross-spectra. Therefore, the commonly used workaround is to discard the microphone auto-spectra, and to process only the cross-spectra.

Figure 4 Set-up with microphone array in DNW-LST closed test section

Another issue in closed test sections is reverberation. When an acoustic source is too close to a wall, the source spectrum reconstructed from array measurements tends to deviate strongly from the free-field source spectrum (Ref. 17). Special techniques (Refs. 18, 19) can be used to correct for this spectral distortion.

The main advantage of closed wind tunnel test sections is that they are more appropriate for aerodynamic measurements. From the acoustics point of view, a great advantage is that coherence is mostly preserved. As a result, sources can be identified at a higher spatial resolution than in open jet wind tunnels, and level estimates are more reliable. Moreover, the preservation of coherence make microphone array measurements in closed wind tunnel test sections very suitable for so-called deconvolution techniques (e.g. Refs. 20-23).
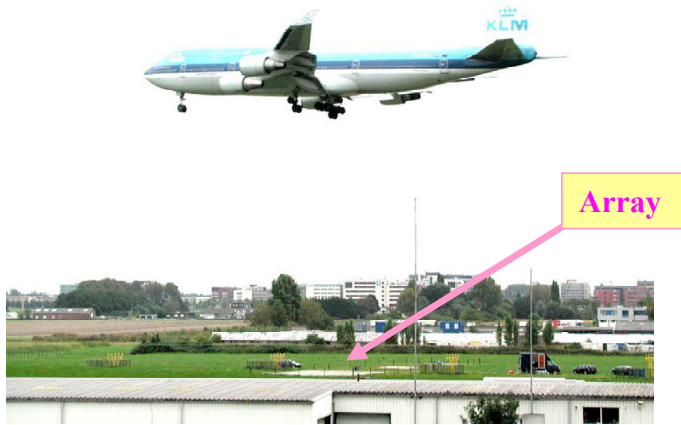
Figure 5 Fly-over microphone array measurements at Amsterdam Schiphol Airport

For fly-over tests (see Figure 5), the main issue is the motion of the acoustic sources, and, consequently, the limited time to perform measurements. Loss of coherence is also an issue, but not to the same extent as in open jet wind tunnels. Source Power Integration (Ref. 24) and deconvolution (Ref. 25) are both feasible.

This paper gives an overview of microphone array beamforming techniques that can be applied in wind tunnels and with fly-over tests. First, some basic principles are discussed. Then, a number of advanced methods are summarised. Finally, one chapter is devoted to processing with moving sources.

2 Basic principles

To obtain source localisation maps or "acoustic images" from microphone arrays measurements, sampled microphone data need to be processed with some beamforming algorithm, under the assumption of a certain source model. This process is done usually in the frequency domain. The basic steps are worked out in this chapter.

2.1 Sampled microphone data

Consider a set of N microphones, located in $\vec{x}_n = (x_n, y_n, z_n)$, where n runs from 1 to N. When the microphone membranes are subject to pressure fluctuations $\chi_n(t)$, an alternating current (AC) is induced, of which the potential (in Volts) is recorded by the data-acquisition system. Contemporary systems are equipped with an analogue/digital (A/D) converter that samples the

15

alternating voltage at a given sample interval Δt, where each sample is stored in a given number of bits (typically 16 or 24). To obtain unsteady (acoustic) pressures

$$\chi_{n,k} = \chi_n(k\Delta t) \tag{1}$$

at the microphone locations, the stored voltages are multiplied with microphone sensitivity factors obtained from calibrations.

2.2   Fourier transformation of microphone data

2.2.1   Discrete Fourier transform

Complex pressure amplitudes $p_n(f)$ of microphone signals can be obtained by evaluating a discrete Fourier transform for a block of K samples:

$$p_n(f) = \frac{2}{K} \sum_{k=1}^{K} \chi_{n,k} e^{-2\pi i f k \Delta t} \; . \tag{2}$$

If the block size K is a power of 2, i.e., if an integer number q exists for which

$$K = 2^q , \tag{3}$$

then the so-called Fast Fourier Transform (FFT; Ref. 26) can be applied to evaluate (2) at once, for the entire relevant range of frequencies, which is (Ref. 27)

$$f_j = \frac{j}{K\Delta t}, \; j = 1, ..., K/2 - 1 . \tag{4}$$

2.2.2   Aliasing

It is noted that the frequency upper limit in (4): $f_{K/2} = \dfrac{1}{2\Delta t}$ equals half the sample frequency:

$$f_{\mathrm{sam}} = 1/\Delta t . \tag{5}$$

In the literature (e.g. Ref. 27), this frequency is called "Nyquist frequency" or "folding frequency". Evaluation of (2) above that frequency does not add anything, because

$$p_n(f) = p_n(f_{\mathrm{sam}} - f)^* , \tag{6}$$

where the asterisk denotes complex conjugation. Thus, frequencies higher than the Nyquist frequency can not be distinguished from their low-frequency counterparts. This is an undesired phenomenon called "aliasing". To avoid aliasing, the acoustic signal should pass through a "low pass filter" that cuts off frequencies above the Nyquist frequency, before entering the A/D converter.

16

2.2.3 Cross-powers

Auto-powers $C_{nn}(f)$ and cross-powers $C_{mn}(f)$ are defined by

$$C_{mn}(f) = \frac{1}{2} p_m(f) p_n^*(f) \,. \tag{7}$$

2.2.4 Relation with cross-spectral density function

The cross-correlation function of the signals from microphones n and m is defined as (Ref. 27)

$$R_{mn}(t) = \lim_{T_0 \to \infty} \frac{1}{T_0} \int_{-T_0/2}^{T_0/2} \chi_m(\tilde{t}) \chi_n(\tilde{t} + t) d\tilde{t} \,. \tag{8}$$

The cross-spectral density function is defined as the Fourier transform of the cross-correlation function:

$$\hat{G}_{mn}(f) = \int_{-\infty}^{\infty} R_{mn}(t) e^{-2\pi i f t} dt = \lim_{T_0 \to \infty} \frac{1}{T_0} \left(\int_{T_0/2}^{T_0/2} \chi_m(t) e^{-2\pi i f t} dt \right)^* \left(\int_{-T_0/2}^{T_0/2} \chi_n(t) e^{-2\pi i f t} dt \right) \,. \tag{9}$$

In real life, we can not evaluate these integrals. We have to start from the assumption that the signals $\chi_n(t)$ are periodic with some period T. Then, the same holds for the cross-correlation $R_{mn}(\tau)$ and equation (9) can be expressed as (Ref. 28)

$$\hat{G}_{mn}(f) = \sum_{j=-\infty}^{\infty} \frac{1}{T} \int_0^T R_{mn}(t) e^{-2\pi i f t} dt \times \delta(f - j/T) \,, \tag{10}$$

where δ is the Dirac-delta function. The periodicity further implies that the limit variable T_0 in (8) can be replaced by T. It follows that (10) can be rewritten as

$$\hat{G}_{mn}(f) = \sum_{j=-\infty}^{\infty} \hat{p}_m^*(f) \hat{p}_n(f) \delta(f - j/T) \,, \tag{11}$$

where

$$\hat{p}_n(f) = \frac{1}{T} \int_0^T \chi_n(t) e^{-2\pi i f t} dt \,. \tag{12}$$

The cross-spectral density function, as defined in (11) is valid for positive as well as for negative frequency f. Usually, only positive frequencies are considered. For that purpose, the "single-sided" cross-correlation function is defined as

$$G_{mn}(f) = 2\hat{G}_{mn}(f), f > 0 \,. \tag{13}$$

We can derive

$$G_{mn}(f) = \frac{1}{2} \sum_{j=1}^{\infty} p_m^*(f) p_n(f) \delta(f - j/T) \,, \tag{14}$$

where

$$p_n(f) = 2\hat{p}_n(f) = \frac{2}{T}\int_0^T \chi_n(t)e^{-2\pi i f t}\,dt\,, \tag{15}$$

which is the continuous version of (2). Thus, we can write for the cross-spectral density

$$G_{mn}(f) = \sum_{j=-\infty}^{\infty} C_{mn}^*(f)\delta\left(f - j/T\right). \tag{16}$$

Note that the cross-powers are defined in terms of the complex conjugate of the cross-spectral density function. This is for convenience in the further analysis.

2.2.5 Windows

For reduction of frequency side-lobes, a "window" u_k, $k = 1,..,K$ (Ref. 29) may be applied to (2):

$$p_n(f) = \frac{2}{K}\sum_{k=1}^{K} u_k \chi_{n,k} e^{-2\pi i f k \Delta t}\,. \tag{17}$$

An often used window is the so-called "Hanning window":

$$u_k = \sin^2\left(\pi k/K\right). \tag{18}$$

The features of this window, and many other windows, can be found in reference 29.

In order to obtain results comparable to a "rectangular window" ($u_k \equiv 1$), the numbers u_k have to be normalised somehow. Correct amplitudes (for tonal noise) are found when

$$\frac{1}{K}\sum_{k=1}^{K} u_k = 1\,. \tag{19}$$

Correct auto- and cross-power levels (for broadband noise) are found when

$$\frac{1}{K}\sum_{k=1}^{K} u_k^2 = 1\,. \tag{20}$$

2.2.6 Averaging

As derived in section 2.2.4, definition (7) for the cross-powers assumes a periodic signal, which is not true for broadband noise. However, if the signal is stationary (statistically expected properties are independent of starting sample), we can average the cross-powers over many blocks of *K* samples. Thus, statistical variations are averaged out.

To minimise numerical errors, the average values should be evaluated as a sequence:

$$\langle C_{mn} \rangle_{\nu} = \left((\nu - 1) \langle C_{mn} \rangle_{\nu-1} + C_{mn,\nu} \right) \Big/ \nu \,. \tag{21}$$

In the sequel of this paper, it will not explicitly be mentioned that cross-powers are the result of averaging.

2.3   Source description

Phased array beamforming is always done using a model that describes the sources characteristics and the propagation from source to receiver. Usually it is assumed that the sound propagates through a medium with uniform flow $\vec{U}$ is assumed. Herein, the acoustic pressure $\chi(\vec{x},t)$ satisfies the convective wave equation:

$$\nabla^2 \chi - \frac{1}{c^2} \left(\frac{\partial}{\partial t} + \vec{U} \cdot \nabla \right)^2 \chi = 0 \,, \tag{22}$$

where c is the speed of sound and ∇ is the "Nabla operator" $\left(\partial/\partial x, \partial/\partial y, \partial/\partial z \right)$. In the frequency-domain Eq. (22) transforms into the convective Helmholtz equation:

$$\nabla^2 p - \frac{1}{c^2} \left(2\pi i f + \vec{U} \cdot \nabla \right)^2 p = 0 \,. \tag{23}$$

2.3.1   Plane waves

If only the direction of the sound is of interest, e.g., if the sound is coming from the far field, then the propagation can be described by plane waves:

$$p(f) = \exp\left[i\vec{\alpha} \cdot \vec{x} \right]. \tag{24}$$

Herein, the wave number vector $\vec{\alpha}$ must satisfy the dispersion relation:

$$\left(2\pi f / c + \vec{M} \cdot \vec{\alpha} \right)^2 - \left\| \vec{\alpha} \right\|^2 = 0 \tag{25}$$

where $\vec{M}$ is a vector of Mach numbers:

$$\vec{M} = \vec{U} \big/ c \,. \tag{26}$$

2.3.2   Point sources

For wind tunnel and fly-over applications, the plane wave model is usually not valid. Instead, a monopole point source description is often used. This is an ideal point source with uniform directivity. In a medium with a uniform flow, its sound pressure field has to satisfy the following partial differential equation:

$$\nabla^2 \chi - \frac{1}{c^2} \left(\frac{\partial}{\partial t} + \vec{U} \cdot \nabla \right)^2 \chi = \sigma(t) \delta(\vec{x} - \vec{\xi}) \,, \tag{27}$$

where $\vec{\xi}$ is the monopole location and $\sigma(t)$ is the emitted signal. The solution of (27) is

$$\chi = \frac{-\sigma\left(t - \Delta t_e\right)}{4\pi\sqrt{\left(\vec{M} \cdot (\vec{x} - \vec{\xi})\right)^2 + \beta^2 \left\|\vec{x} - \vec{\xi}\right\|^2}} \; , \tag{28}$$

where Δt_e is the emission time delay:

$$\Delta t_e = \frac{1}{c\beta^2}\left(-\vec{M} \cdot (\vec{x} - \vec{\xi}) + \sqrt{\left(\vec{M} \cdot (\vec{x} - \vec{\xi})\right)^2 + \beta^2 \left\|\vec{x} - \vec{\xi}\right\|^2}\right) \tag{29}$$

and

$$\beta^2 = 1 - \left\|\vec{M}\right\|^2 . \tag{30}$$

The frequency-domain version of (28) reads

$$p = \frac{-a e^{-2\pi i f \Delta t_e}}{4\pi\sqrt{\left(\vec{M} \cdot (\vec{x} - \vec{\xi})\right)^2 + \beta^2 \left\|\vec{x} - \vec{\xi}\right\|^2}} \; , \tag{31}$$

where a is the Fourier transform of σ.

Dipoles, quadrupoles, and all sorts of combinations (multipoles) are possible too, simply by considering partial derivatives of (31). For microphone arrays, this usually does not add much to the monopole description, because the array covers often only a small portion of the solid angle of the directivity pattern of a source. Then, the source will be detected as if it were a monopole.

Occasionally, "dipole beamforming" has added value (Ref. 30).

2.3.3 Corrections for wind tunnel shear layer

Obviously, the assumption of uniform flow is not valid in the case of out-of-flow measurements in an open jet wind tunnel. In that case, the effect of transmission through the shear layer has to be incorporated in the source description.

A simple, but effective way of incorporating this in the source description (31) is to replace the uniform flow Mach number by the average Mach number between source and microphone. For instance, if the wind tunnel shear layer is defined by $z = z_{sl}$ and $\vec{M} = M\vec{e}_x$, then the corrected Mach number is given by

$$M_{\mathrm{cor}} = M\frac{\zeta - z_{sl}}{\zeta - z} , \tag{32}$$

where z and ζ are the z-co-ordinates of $\vec{x}$ and $\vec{\xi}$, respectively.

This shear layer correction, which may seem a little crude, has been extensively compared with two more sophisticated methods: the Amiet correction (Ref. 31) for an infinitely thin shear layer and ray acoustics (Ref. 32) incorporating the finite thickness of the shear layer. This comparison was done through microphone array simulations with a point source. It revealed that the differences in array output between the three methods were negligible, as long as the Mach number is moderate (say $M \leq 0.25$) and the angles between the shear layer and the acoustic rays are not too small (say $\geq 45°$).

2.4 Conventional Beamforming

From now on, we will write the array-related quantities as *N*-dimensional vectors and matrices. Furthermore, for brevity, we will omit the frequency dependence $"(f)"$. This means that the "pressure amplitudes",(2) are put in an *N*-dimensional vector $\mathbf{p}$:

$$\mathbf{p} = \begin{pmatrix} p_1(f) \\ \vdots \\ p_N(f) \end{pmatrix}.$$
(33)

Furthermore, the cross-power matrix $\mathbf{C}$ is introduced by

$$\mathbf{C} = \frac{1}{2}\mathbf{p}\mathbf{p}^*,$$
(34)

where the asterisk means "complex conjugate transpose". The source description is put in the "steering vector" $\mathbf{g}$, i.e., its components g_n are the pressure amplitudes at the microphone locations of an ideal source with unit strength. For instance, in the case of a monopole in a medium with uniform flow, we have (Eq. (31))

$$g_n = \frac{-e^{-2\pi i f \Delta t_e(\vec{x}_n, \vec{\xi})}}{4\pi\sqrt{\left(\vec{M} \cdot (\vec{x}_n - \vec{\xi})\right)^2 + \beta^2 \left\|\vec{x}_n - \vec{\xi}\right\|^2}}.$$
(35)

The purpose of beamforming is to determine complex amplitudes *a* of sources in $\vec{\xi}$. This is done by comparing the measured pressure vector $\mathbf{p}$ with the steering vector $\mathbf{g}$, for instance through minimisation of

$$J = \left\|\mathbf{p} - a\mathbf{g}\right\|^2.$$
(36)

The solution of this minimisation problem is

$$a = \frac{\mathbf{g}^*\mathbf{p}}{\left\|\mathbf{g}\right\|^2}.$$
(37)

21

In the case of broadband noise, it does not make sense to apply averaging (Section 2.2.6) to expression (37), because its phase will be different for each block. Then, it is more convenient to consider source auto-powers:

$$A = \frac{1}{2}|a|^2 = \frac{1}{2}aa^* = \frac{1}{2}\frac{\mathbf{g}^*\mathbf{p}}{\|\mathbf{g}\|^2}\left(\frac{\mathbf{g}^*\mathbf{p}}{\|\mathbf{g}\|^2}\right)^* = \frac{1}{2}\frac{\mathbf{g}^*\mathbf{pp}^*\mathbf{g}}{\|\mathbf{g}\|^4} = \frac{\mathbf{g}^*\mathbf{Cg}}{\|\mathbf{g}\|^4} . \tag{38}$$

Expression (38) is known as "Conventional Beamforming".

Source cross-powers $A_{1,2}$ of two different source locations $\vec{\xi}_1$ and $\vec{\xi}_2$ (described by steering vectors $\mathbf{g}_1$ and $\mathbf{g}_2$) can be considered also:

$$A_{1,2} = \frac{1}{2}a_1a_2^* = \frac{1}{2}\frac{\mathbf{g}_1^*\mathbf{p}}{\|\mathbf{g}_1\|^2}\frac{\mathbf{p}^*\mathbf{g}_2}{\|\mathbf{g}_2\|^2} = \frac{\mathbf{g}_1^*\mathbf{Cg}_2}{\|\mathbf{g}_1\|^2\|\mathbf{g}_2\|^2} . \tag{39}$$

3 Array Performance

3.1   Example with random array

3.1.1   Beam pattern

In this section, simulations are carried out with a planar array of 50 microphones positioned randomly on a disk of 2 m radius, in the plane $z = 0$. The microphone locations are shown in Figure 6. A monopole source is simulated 6 m above the array, in $(0,0,6)$. The frequency of the emitted sound is 2000 Hz. Using the Conventional Beamforming technique, an acoustic scan was made on a surface of 4×4 m², 6 m above the array. The result of this scan, i.e., the "source plot" or the "acoustic image" is shown in Figure 7. Such a source plot of a single source is called "beam pattern". The results are presented in dB; the dynamic range of the plot (i.e., the range of the colour bar) is 16 dB.
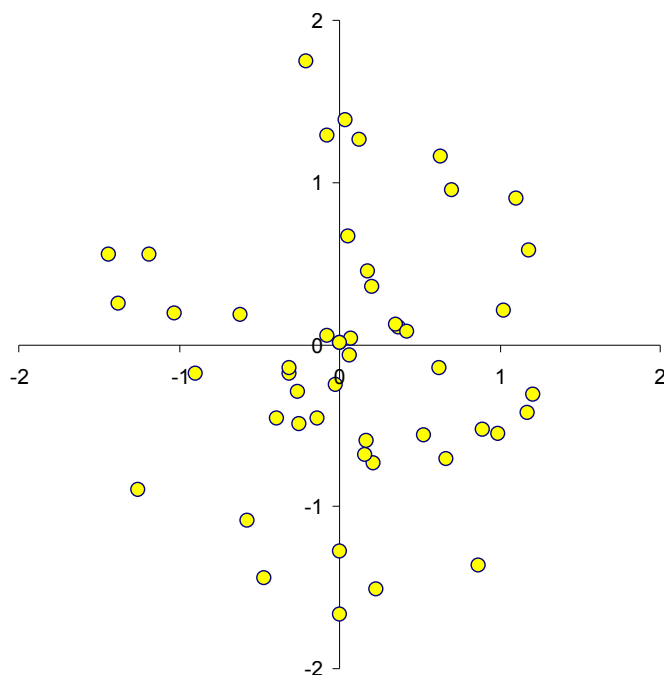
Figure 6 Random array of 50 microphones

3.1.2   Main lobe

In the centre of Figure 7, the source location can be recognised as the peak location. In the neighbourhood of the peak location, the estimated levels decrease with increasing distance from the source. Thus, a lobe appears: the so-called "main lobe" of the beam pattern. The width of the main lobe is a measure of the resolution of the array. Usually (Ref. 33), the resolution is defined as the width of the main lobe, 3 dB below its peak (see Figure 8).

The resolution of an array depends on its size, on frequency, on distance to the source, on the individual microphone locations, and on the used beamforming algorithm. With Conventional Beamforming, a rule of thumb for the resolution of an array is

$$\text{Resolution} = \frac{425Y}{Df},$$
(40)

where Y is the distance between source and array, and D is the diameter of the array. In the example of Figure 7, the resolution is 38 cm, whereas the rule of thumb (40) yields 32 cm.
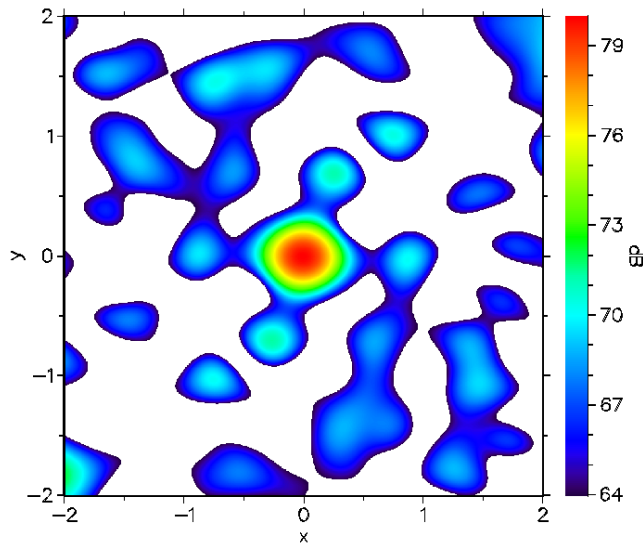
Figure 7 Source plot (at z = 6) with random array (at z = 0), f = 2000 Hz
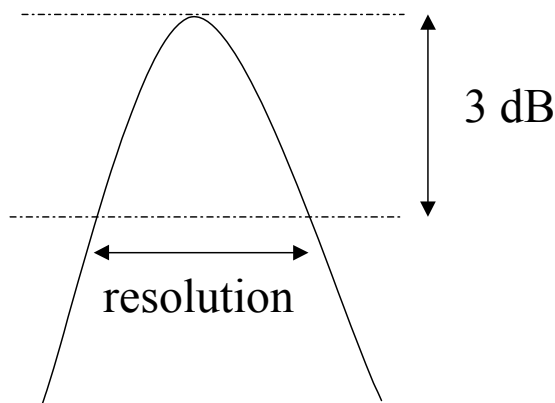
Figure 8 Definition of array resolution

3.1.3   Side lobes

Apart from the main lobe, the beam pattern (Figure 7) also consists of "side lobes", i.e., local peaks. These side lobes are inevitable, due to the finite number of microphones. Since it is difficult to distinguish between the side lobes of a main source and the main lobe of a secondary source, it is desirable to keep the side lobe levels as low as possible. This is one of the main concerns in the design of a microphone layout (Refs. 34, 35).

A measure for the array performance is its "dynamic range" or "array gain", which is defined as the difference between the peak level and the highest side lobe level of a beam pattern. This dynamic range depends on the number of microphones, microphone layout, source location, scan grid, frequency and beamforming algorithm. The array gain of the example shown in Figure 7 is 8.5 dB.

3.2 Improvement of microphone layout

3.2.1 Aperture smoothing function

The issue of side lobes can be understood by considering far-field beamforming, i.e., by using the source model (24). Suppose that the incoming plane wave is described by

$$p(\vec{x}) = \exp\left[i\vec{\alpha}_0 \cdot \vec{x}\right]. \tag{41}$$

Then, the Conventional Beamforming algorithm (37) yields

$$a = \frac{1}{N}\sum_{n=1}^{N}\exp\left[i\left(\vec{\alpha}_0 - \vec{\alpha}\right)\cdot\vec{x}_n\right]. \tag{42}$$

Expression (42) can be written as

$$a = W\left(\vec{\alpha}_0 - \vec{\alpha}\right), \tag{43}$$

where W is the "aperture smoothing function" (see also Ref. 14):

$$W(\vec{\alpha}) = \frac{1}{N}\sum_{n=1}^{N}\exp\left[i\vec{\alpha}\cdot\vec{x}_n\right]. \tag{44}$$

The ideal array should have an aperture smoothing function satisfying

$$\begin{cases} W(\vec{0}) = 1 \\ W(\vec{\alpha}) = 0, \text{ for } \vec{\alpha} \neq \vec{0} \end{cases} \tag{45}$$

However, with a finite number of microphones this is impossible. The local peak values of W for $\vec{\alpha} \neq \vec{0}$ represent side lobes.

3.2.2 Reduction of side lobes by array design

A possibility to reduce side lobe levels is to minimise, as a function of microphone locations, the following expression:

$$J\left(\vec{x}_1,...,\vec{x}_N\right) = \iiint\limits_{\alpha_{\min}\leq\|\vec{\alpha}\|\leq\alpha_{\max}}\left|W(\vec{\alpha})\right|^2 \mathrm{d}\,\vec{\alpha} = \frac{1}{N^2}\iiint\limits_{\alpha_{\min}\leq\|\vec{\alpha}\|\leq\alpha_{\max}}\left|\sum_{n=1}^{N}\exp\left[i\vec{\alpha}\cdot\vec{x}_n\right]\right|^2 \mathrm{d}\,\vec{\alpha}. \tag{46}$$

The bounds $\alpha_{\min}$ and $\alpha_{\max}$ depend on the array requirements. In practice, $\alpha_{\min}$ depends on the array diameter, and $\alpha_{\max}$ on the maximum frequency.

For a two-dimensional (planar) array, we can analogously minimise

$$J\left(x_1,...,x_N,y_1,...,y_N\right) = \frac{1}{N^2}\iint\limits_{\alpha_{\min}^2\leq\alpha_x^2+\alpha_y^2\leq\alpha_{\max}^2}\left|\sum_{n=1}^{N}\exp\left[i\left(\alpha_x x_n + \alpha_y y_n\right)\right]\right|^2 \mathrm{d}\alpha_x\,\mathrm{d}\alpha_y. \tag{47}$$

25

Practical choices for α_{min} and α_{max} are

$$\alpha_{min} = \frac{3.83}{D}, \tag{48}$$

$$\alpha_{max} = \pi \frac{f_{max}}{c}, \tag{49}$$

where f_{max} is the maximum frequency to be analysed.

Expression (47) can be evaluated as

$$
\begin{aligned}
J\left(x_1,...,x_N, y_1,...,y_N\right) \\
= \frac{1}{N^2} \sum_{m=1}^{N} \sum_{n=1}^{N} \iint_{\alpha_{min}^2 \leq \alpha_x^2 + \alpha_y^2 \leq \alpha_{max}^2} \exp\left[i\left(\alpha_x(x_m - x_n) + \alpha_y(y_m - y_n)\right)\right] \mathrm{d}\alpha_x \, \mathrm{d}\alpha_y \\
= \frac{1}{N^2} \sum_{m=1}^{N} \sum_{n=1}^{N} \int_{\alpha_{min}}^{\alpha_{max}} r \int_{0}^{2\pi} \exp\left[ird_{mn}\cos(\theta)\right] \mathrm{d}\theta \, \mathrm{d}r,
\end{aligned} \tag{50}
$$

in which

$$d_{mn}^2 = (x_m - x_n)^2 + (y_m - y_n)^2. \tag{51}$$

Using some properties of Bessel functions (Ref. 36), we can evaluate (50) further as

$$
\begin{aligned}
J\left(x_1,...,x_N, y_1,...,y_N\right) &= \frac{1}{N^2} \sum_{m=1}^{N} \sum_{n=1}^{N} \int_{\alpha_{min}}^{\alpha_{max}} 2\pi r J_0(rd_{mn}) \, \mathrm{d}r \\
&= \frac{\pi}{N^2} \left\{ \sum_{n=1}^{N} \int_{\alpha_{min}}^{\alpha_{max}} 2r \, \mathrm{d}r - 2\sum_{m=1}^{N} \sum_{\substack{n=1 \\ m \neq n}}^{N} \frac{1}{R_{mn}} \int_{\alpha_{min}}^{\alpha_{max}} \frac{\mathrm{d}}{\mathrm{d}r}\left(rJ_0'(rd_{mn})\right) \mathrm{d}r \right\} \\
&= \frac{\pi}{N^2} \left\{ N\left(\alpha_{max}^2 - \alpha_{min}^2\right) - 2\sum_{m=1}^{N} \sum_{\substack{n=1 \\ m \neq n}}^{N} \frac{\alpha_{max} J_0'(\alpha_{max} d_{mn}) - \alpha_{min} J_0'(\alpha_{min} d_{mn})}{d_{mn}} \right\},
\end{aligned} \tag{52}
$$

in which J_0 is the zero-th order Bessel function of the first kind. Expression (52) can be minimised as a function of the parameters x_n and y_n. Since the derivatives of J can be evaluated analytically, this minimisation can be done relatively quickly by using, for example, the Conjugate Gradient Method (Ref. 26).

3.2.3   Example with optimised array

Using the optimisation procedure described in Section 3.2.2 and the random array of Figure 6 as starting positions, an optimised array was calculated. The result is shown in Figure 9. With this optimised array, the same simulation was carried out as in Section 3.1.1. The beam pattern of

the simulated source is shown in Figure 10. Compared to the result with the random array (Figure 7), the resolution (width of main lobe) is virtually the same. However the side lobe levels are clearly lower. Instead of 8.5 dB in Figure 7, the array gain is now 12.5 dB.
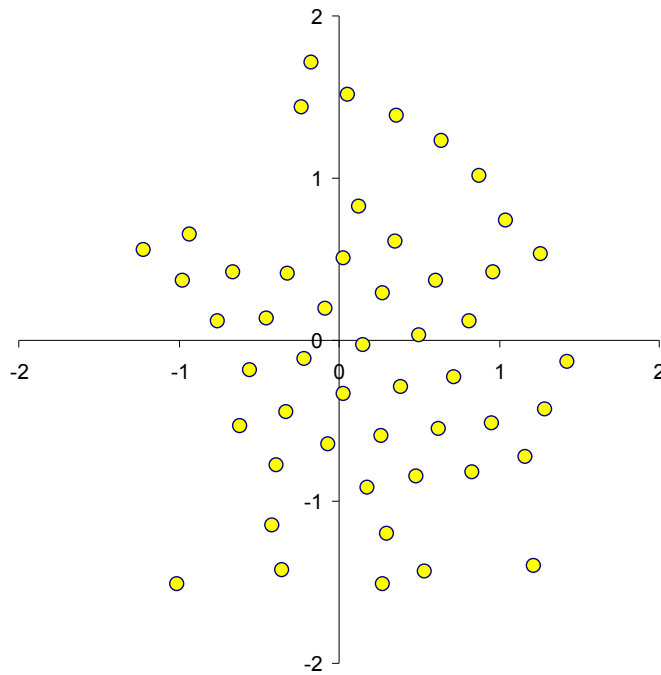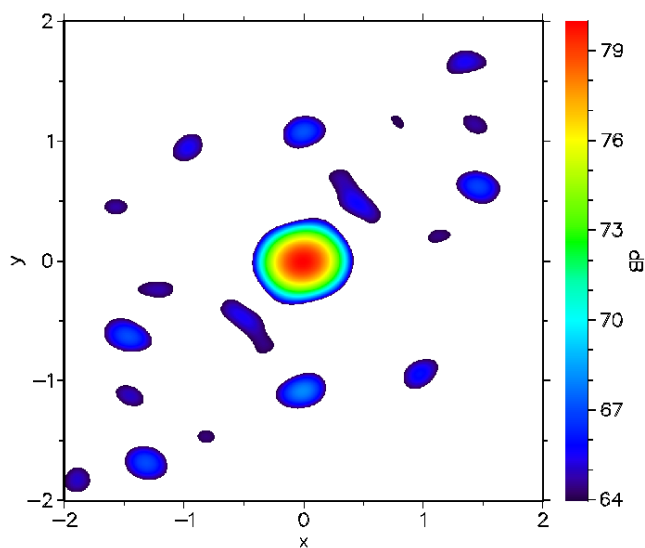

Figure 9 Optimised array

Figure 10 Source plot with optimised array, f = 2000 Hz

4 Advanced methods

4.1 Microphone weights

It is possible to apply weight factors v_n, i.e. a spatial window, to the microphones. These weights may be frequency-dependent. Each of the beamforming methods described in this report can be applied using microphone weight factors, when the cross-powers C_{mn} are replaced by $v_m v_n C_{mn}$ and the steering vector components g_n by $v_n g_n$.

The weight factors v_n may be the product of two separate weights:

$$v_n = \lambda_n \mu_n, \tag{53}$$

where λ_n is a weight to correct for the microphone density and μ_n is a frequency-dependent weight to correct for the effective aperture of the array. This is worked out in the following.

4.1.1 Corrections for microphone density

The weights λ_n are chosen such that the acoustic power per unit area is approximately constant. This means that λ_n is large for sparsely spaced microphones, typically at the periphery of the array, and that λ_n is small at the centre of the array, where the microphones are densely spaced. In mathematics (see also Figure 11):

$$\sum \left\{ \lambda_n^2; \ \vec{x}_n \in \Omega \right\} \Big/ \text{area}(\Omega) \approx \text{Constant} \ (\text{independent of } \Omega) . \tag{54}$$

The effect of the application of such weight factors is that less emphasis is put on the central part of the array, and hence that the spatial resolution is enlarged. The resolution is then comparable to the resolution of a continuous disk (or elliptic mirror) of the same aperture.
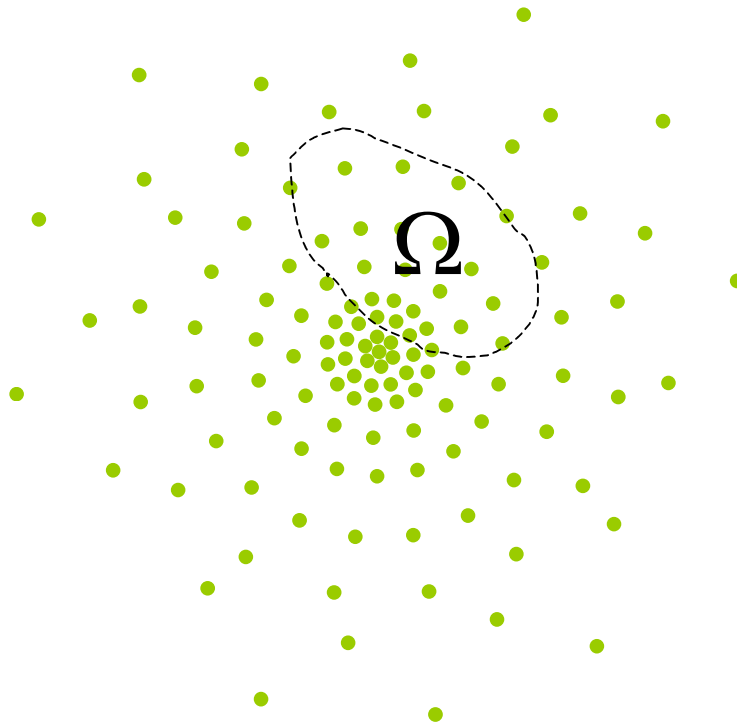
Figure 11 Illustration of equation (54)

4.1.2   Corrections for effective aperture

If the incoming sound is affected by coherence loss, then the signals of the outer, sparsely spaced microphones are incoherent with signals of other microphones. Hence, these outer microphones do not contribute effectively to the beamforming process. As a result, the effective array size may be much smaller than the physical size and the peak values in the source localisation maps may be much too low.

The weights μ_n are used to correct for the effective aperture of the array. Inner microphones will get high values of μ_n and outer microphones low values. The effect is that less noise is visible in the source maps and that the peak values are more realistic. Moreover, these weights can be used to control the lobe width.

The following expression is used (see also Figure 12):

$$\mu_n(f) = \frac{1}{2}\left\{1 - \text{Erf}\left[8\left(\frac{r_n}{R(f)} - 1\right)\right]\right\}, \tag{55}$$

where 'Erf' is the Error function, r_n the distance to the midpoint of the array:

$$r_n = \left\| \vec{x}_n - \frac{1}{N} \sum_{m=1}^{N} \vec{x}_m \right\|, \tag{56}$$

and $R(f)$ the frequency-dependent 'aperture radius'. We assume that $R(f)$ is proportional to the wave length, hence inversely proportional to the frequency:

$$R(f) = B/f . \tag{57}$$
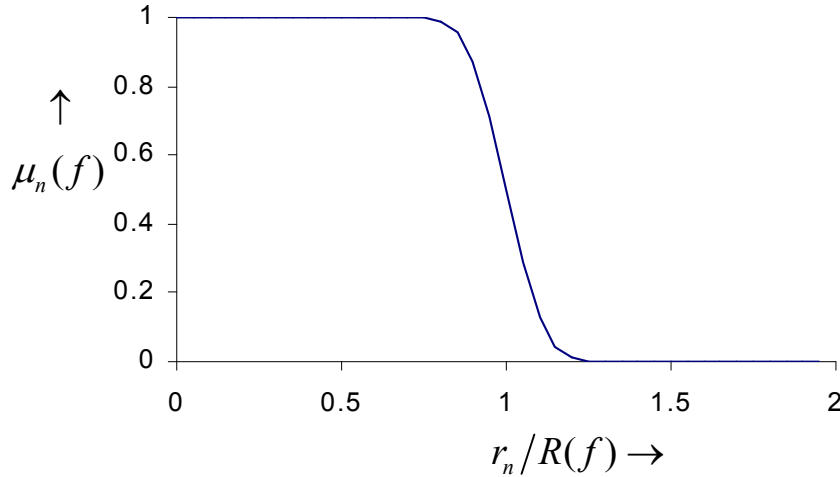
Figure 12 Illustration of equation (55)

4.2   Beamforming without auto-spectra

In wind tunnel measurements, microphone auto-power levels are often much higher than the corresponding cross-power levels. In other words, the main diagonal components of the cross-power matrix **C** have much higher levels than the off-diagonal components. There can be two reasons for this phenomenon, both of which are discussed below.

4.2.1   Boundary layer noise

When a microphone is placed in the wind, it will detect not only acoustic pressures, but also pressure disturbances of hydrodynamic nature due to the turbulent boundary layer around the microphone. This typically occurs in closed wind tunnel test sections, where the microphones are mounted flush in a wall. Because wind noise is incoherent from one microphone to the other (except when microphones are placed very close to each other in the wind direction, and then only for very low wave numbers), it will appear only in the auto-spectra, and not in the cross-spectra.

In mathematics: suppose that the pressure vector **p** is composed of an acoustic component $\mathbf{p}_a$ and a wind noise component $\mathbf{p}_w$. Then for the cross-power matrix we have

30

$$\mathbf{C} = \frac{1}{2}\left(\mathbf{p}_a + \mathbf{p}_w\right)\left(\mathbf{p}_a^* + \mathbf{p}_w^*\right) = \frac{1}{2}\mathbf{p}_a\mathbf{p}_a^* + \frac{1}{2}\mathbf{p}_a\mathbf{p}_w^* + \frac{1}{2}\mathbf{p}_w\mathbf{p}_a^* + \frac{1}{2}\mathbf{p}_w\mathbf{p}_w^*. \qquad (58)$$

The second and the third term in the right hand side disappear through averaging, and what remains is

$$\mathbf{C} = \frac{1}{2}\mathbf{p}_a\mathbf{p}_a^* + \frac{1}{2}\mathbf{p}_w\mathbf{p}_w^* = \mathbf{C}_a + \mathbf{C}_w \qquad (59)$$

The wind noise induced matrix $\mathbf{C}_w$ has, in the limit, only non-zero components on the main diagonal.

4.2.2 Loss of coherence

When sound travels through a turbulent medium, it deforms. When sound from a noise source travels along different paths through a turbulent medium, it will deform differently. As a result, the phase of the cross-power between two microphones will be distorted. Therefore, after averaging, the cross-power levels are lower than in the non-deformed case. This reduction of cross-power level is dependent on the level of the turbulence, the distance between the microphones, the distance between source and microphone and on frequency. Since auto-powers do not contain phase information, their levels are not affected by coherence loss. Hence, auto-powers tend to dominate the cross-power matrix when coherence loss becomes significant.

Loss of coherence is in particular an important issue for measurements in an open jet wind tunnel (Ref. 15), when the array is placed out of the flow and the sound has to travel through the turbulent shear layer. Typically, it makes source location impossible for frequencies higher than 20 kHz. Loss of coherence is also an issue for outdoor measurements (Refs. 37-39), for instance the fly-over measurements at Schiphol Airport (Refs. 10, 24). For those measurements, the turbulence in the atmospheric boundary layer is to blame.

4.2.3 Elimination of auto-powers

In the cases where the auto-powers prevail against the cross-powers, much "cleaner" noise maps are obtained when the auto-powers are not used in the beamforming process. For that purpose, we can generalise the Conventional Beamforming method of Section 2.4 as follows.

Instead of (36), we can equivalently minimise

$$J = \left\|\mathbf{C} - A\mathbf{g}\mathbf{g}^*\right\|^2 = \sum_{m=1}^{N}\sum_{n=1}^{N}\left|C_{mn} - Ag_mg_n^*\right|^2. \qquad (60)$$

This can be generalised into

$$J = \sum_{(m,n)\in S} \left| C_{mn} - A g_m g_n^* \right|^2 , \tag{61}$$

where S is a sub-set of all possible (m,n)-combinations. For instance in case of auto-power elimination, we have

$$S = \left\{ (m,n) \in [1...N] \times [1...N]; m \neq n \right\} . \tag{62}$$

The solution of minimising (61) is

$$A = \frac{\displaystyle\sum_{(m,n)\in S} g_m^* C_{mn} g_n}{\displaystyle\sum_{(m,n)\in S} \left| g_m \right|^2 \left| g_n \right|^2} . \tag{63}$$

A caution to this method is that the source auto-power A, as calculated by (63) may have a negative value, because the governing matrix is not positive-definite anymore. Since negative auto-powers are not physical, those results should be rejected.

Source cross-powers $A_{1,2}$ (see section 2.4) can be found likewise, through minimising

$$J = \sum_{(m,n)\in S} \left| C_{mn} - A_{1,2} g_{1,m} g_{2,n}^* \right|^2 . \tag{64}$$

The solution is

$$A_{1,2} = \frac{\displaystyle\sum_{(m,n)\in S} g_{1,m}^* C_{mn} g_{2,n}}{\displaystyle\sum_{(m,n)\in S} \left| g_{1,m} \right|^2 \left| g_{2,n} \right|^2} . \tag{65}$$

4.2.4 Example

The strength of beamforming without auto-spectra is illustrated by array measurements in the DNW-LST on a half model of the Fokker 100 aircraft (Figure 4). These measurements were used to test flap tip devices (Ref. 40). An array of 96 microphones was used, mounted flush in the wall (red surface in Figure 4). In Figure 13 typical results are shown of beamforming with and without auto-powers. The necessity of beamforming without auto-powers in this situation is clearly demonstrated.
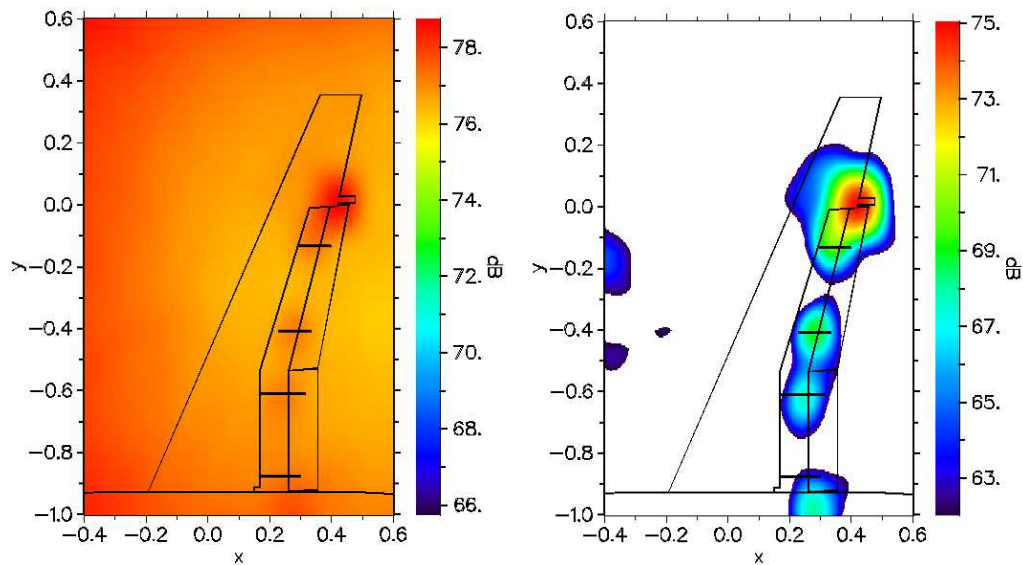
Figure 13 Source plots of Fokker 100 half model; comparison between beamforming with (left) and without (right) auto-powers

4.3   Source Power Integration

Using Conventional Beamforming, absolute source powers can be extracted from array measurements only under the following restrictions:

- The sources are point sources.
- The source directivity is uniform, at least in the direction of the array.
- The resolution of the beamforming method is high enough to separate different sources.
- There is no loss of coherence.

If the requirements above are fulfilled then the source powers can be found as the (local) peak values in the acoustic source plots.

However, in wind tunnel measurements these requirements are seldom fulfilled. To obtain absolute levels nonetheless, a source power integration technique was developed (Refs. 16). Basically, the integration technique sums the source auto-power estimates for all points of a scan grid. Afterwards, the result is scaled such that the exact result is obtained for a simulated point source in the centre of the grid.

For successful application of the integration technique, Conventional Beamforming should be used for the source auto-power estimates. Conventional Beamforming including auto-powers (Section 2.4) is preferred. Conventional Beamforming without auto-powers (Section 4.2) is possible too, however some caution is need. Both methods are discussed below.

The source power integration technique can be applied also to sub-sets of the scan grid. Thus, the source power contributions from several parts of a research model can easily be compared.

4.3.1 Standard method

Suppose H is the number of points in a scan grid, and $A_{s,h}$, $h=1,...H$ are the beamforming results (source auto-power estimates) of a simulated point source in the middle of the grid, with source auto-power P_s. Suppose further that A_h, $h=1,...H$ are the beamforming results from measurements. Then, the integrated source power estimate is

$$P = \frac{\sum_{h=1}^{H} A_h}{\sum_{h=1}^{H} A_{s,h}} \times P_s \tag{66}$$

For several wind tunnel array measurements, reference 16 reported good agreement with levels of individual microphones. Reference 16 also discusses a more advanced integration method, using several reference sources instead of one. Usually, the standard method is applied.

4.3.2 Method without auto-powers

Because of the relatively high auto-power levels in wind tunnel measurements, it is convenient to have available also an integration procedure without auto-powers. However, straightforward application of (66) may lead to poor results. The source auto-power estimates A_h and $A_{s,h}$ can be both positive and negative, which makes expression (66) unstable. A good alternative is to consider only the positive source auto-power estimates:

$$P = \frac{\sum_{h=1}^{H} \max(A_h,0)}{\sum_{h=1}^{H} \max(A_{s,h},0)} \times P_s . \tag{67}$$

The following, more refined method considers only the source auto-power estimates that are less than Z dB (typically 10 dB) below the peak levels $A_{\max}$ and $A_{s,\max}$. In other words, power estimates that are more than Z dB below the peak values are neglected. Thus, we have for the integrated source power

$$P = \frac{\sum_{h=1}^{H} \tilde{A}_h}{\sum_{h=1}^{H} \tilde{A}_{s,h}} \times P_s , \tag{68}$$

where

34

$$\tilde{A}_h = \begin{cases} 0, \text{ if } A_h \leq 0 \text{ or } 10^{10}\log\left(A_h/A_{\max}\right) \leq -Z, \\ A_h, \text{ otherwise,} \end{cases} \tag{69}$$

and

$$\tilde{A}_{s,h} = \begin{cases} 0, \text{ if } A_{s,h} \leq 0 \text{ or } 10^{10}\log\left(A_{s,h}/A_{s,\max}\right) \leq -Z, \\ A_{s,h}, \text{ otherwise.} \end{cases} \tag{70}$$

The integration method without auto-power loses its ability to predict correct levels when coherence loss becomes significant. This is especially the case in open jet wind tunnels. This technique is, nevertheless, still convenient as a tool to compare different integration areas and different model configurations.

4.4 The use of eigenvalue analysis

An other useful technique that can be applied when auto-powers are not dominating, is an eigenvalue decomposition of the cross-power matrix. Herewith, the measured acoustic pressure can be split into incoherent "principal" components. This technique can be used for

   a) determining the number of incoherent sources,
   b) increasing the processing speed,
   c) noise filtering.

Successful applications of this technique are described in references 17 and 42. The analysis is as follows.

Suppose there are L independent sources:

$$\mathbf{p} = \sum_{l=1}^{L} \mathbf{p}_l \,. \tag{71}$$

For the cross-power matrix, we have

$$\mathbf{C} = \frac{1}{2}\left(\sum_{l=1}^{L}\mathbf{p}_l\right)\left(\sum_{l=1}^{L}\mathbf{p}_l\right)^* = \frac{1}{2}\sum_{l_1=1}^{L}\sum_{l_2=1}^{L}\mathbf{p}_{l_1}\mathbf{p}_{l_2}^* \,. \tag{72}$$

After averaging, the following expression remains:

$$\mathbf{C} = \frac{1}{2}\sum_{l=1}^{L}\mathbf{p}_l\mathbf{p}_l^* \,. \tag{73}$$

Herewith, $\mathbf{C}$ is a matrix with rank L. In other words, the number of non-zero eigenvalues of $\mathbf{C}$ is equal to the number of incoherent sources. Since the matrix $\mathbf{C}$ is Hermitian (invariant to complex conjugate transposition) and positive definite, its eigenvalues are non-negative and the corresponding eigenvectors form an orthogonal set. The eigenvectors of $\mathbf{C}$ or "principal

components" correspond to virtual sources, which need not coincide with the physical incoherent sources.

The cross-power matrix $\mathbf{C}$ can be written as

$$\mathbf{C} = \mathbf{QEQ}^*, \tag{74}$$

where $\mathbf{E}$ is an $L \times L$ diagonal matrix containing the non-zero eigenvalues, and $\mathbf{Q}$ is an $N \times L$ matrix, the columns of which are the normalised eigenvectors of $\mathbf{C}$. For the Conventional Beamforming algorithm (38) we then have

$$A = \frac{\mathbf{g}^*\mathbf{QEQ}^*\mathbf{g}}{\|\mathbf{g}\|^4}. \tag{75}$$

In general, the matrix $\mathbf{C}$ will <u>not</u> have a number (L) of non-zero and a number ($N-L$) of zero eigenvalues. The reality will be that $\mathbf{C}$ has a full spectrum. If the signal-to-noise ratio is sufficiently high, then the signals can be recognised in the space spanned by the eigenvectors corresponding to the highest eigenvalues. In other words, if a number of eigenvalues has significantly higher values than the rest, they can be attributed to incoherent sources. The lower eigenvalues represent noise, which can be filtered out by replacing the lowest eigenvalues by zero.

When one principal component is dominant, we can enlarge the dynamic range of the array by filtering this component out, viz. removing from the cross-power matrix the eigenvector corresponding to the highest eigenvalue (Ref. 41).

4.5 Deconvolution using CLEAN

4.5.1 Traditional CLEAN

An other method of removing a dominant source is CLEAN (Ref. 43), a technique that astronomers use to remove side lobes of bright stars from maps obtained with multiple telescopes. Basically, CLEAN performs the following steps

- It searches for the location of the maximum source auto-power in the acoustic image.
- It subtracts the appropriately scaled theoretical beam pattern of that source ("dirty beam", including side lobes) from the acoustic image.
- It replaces this "dirty beam" by a "clean beam" (beam without side lobes).

This process can be done iteratively, for multiple sources. Ignoring the issue of constructing "clean beams", the analysis is as follows.

First, we express the Conventional Beamforming expression (38) as

$$A = \mathbf{w}^*\mathbf{C}\mathbf{w}, \tag{76}$$

where $\mathbf{w}$ is the "weight vector":

$$\mathbf{w} = \frac{\mathbf{g}}{\|\mathbf{g}\|^2}. \tag{77}$$

Suppose that $\mathbf{w}_{\max}$ is the weight vector with the maximum array output $A_{\max}$:

$$A_{\max} = \mathbf{w}_{\max}^* \mathbf{C}\mathbf{w}_{\max}. \tag{78}$$

The weight vector $\mathbf{w}_{\max}$ points to a source location $\vec{\xi}_{\max}$, to which a steering vector $\mathbf{g}_{\max}$ is associated. A modified array output A_{mod}, without the disturbing influence of the source in $\vec{\xi}_{\max}$ can formally be written as

$$A_{\mathrm{mod}} = \mathbf{w}^*\mathbf{C}\mathbf{w} - \mathbf{w}^*\mathbf{C}_{\max}\mathbf{w}, \tag{79}$$

where $\mathbf{C}_{\max}$ is the cross-power matrix induced by the source in $\vec{\xi}_{\max}$. This matrix $\mathbf{C}_{\max}$ is unknown, but a reasonable guess seems to be

$$\mathbf{C}_{\max} = A_{\max}\mathbf{g}_{\max}\mathbf{g}_{\max}^*. \tag{80}$$

Equations (79) and (80) form the basis for the CLEAN algorithm, which is as follows:

Step 1:   Apply the beamforming algorithm to the scan plane, search for the peak source location $\vec{\xi}_{\max}$, and determine the corresponding matrix $\mathbf{C}_{\max}$.

Step 2:   Replace the cross-power matrix $\mathbf{C}$ by $\mathbf{C} - \varphi\mathbf{C}_{\max}$, where φ is a safety factor with $0 < \varphi \le 1$, called the "loop gain".

Step 3:   Return to step 1, unless a certain stop criterion is fulfilled.

Afterwards, the information that has been subtracted in Step 2 can be used to produce a "clean map".

A good stop criterion could be $\mathrm{norm}(\mathbf{C} - \varphi\mathbf{C}_{\max}) \ge \mathrm{norm}(\mathbf{C})$, where the norm is defined by

$$\mathrm{norm}(\mathbf{C}) = \sum_{n=1}^{N}\sum_{m=1}^{N}\left|C_{nm}\right|. \tag{81}$$

The CLEAN algorithm, as sketched above, is based on the assumption of point sources. Furthermore, it assumes that the sound transfer is well described by $\mathbf{g}_{\max}$. The latter assumption includes a uniform directivity and no loss of coherence, which is seldom fulfilled in aero-acoustic measurements.

To overcome this limitation, alternative approximations for $\mathbf{C}_{\max}$ are proposed below, which form the basis of the CLEAN-SC method (Ref. 23).

37

4.5.2 CLEAN-SC

In CLEAN-SC, the matrix $\mathbf{C}_{\max}$ is defined such that the source cross-power (cf. Eq. (39)) of any scan point $\vec{\xi}$ with the peak location $\vec{\xi}_{\max}$ is determined entirely by $\mathbf{C}_{\max}$. In other words,

$$\mathbf{w}^* \mathbf{C} \mathbf{w}_{\max} = \mathbf{w}^* \mathbf{C}_{\max} \mathbf{w}_{\max}, \text{ for all possible } \mathbf{w}. \tag{82}$$

This is satisfied when

$$\mathbf{C} \mathbf{w}_{\max} = \mathbf{C}_{\max} \mathbf{w}_{\max}. \tag{83}$$

Equation (83) does not have a unique solution for $\mathbf{C}_{\max}$, but it does when we write

$$\mathbf{C}_{\max} = A_{\max} \mathbf{h} \mathbf{h}^*. \tag{84}$$

The solution of (83) with (84) is

$$\mathbf{h} = \frac{\mathbf{C} \mathbf{w}_{\max}}{A_{\max}}, \tag{85}$$

and, consequently,

$$\mathbf{C}_{\max} = \frac{\mathbf{C} \mathbf{w}_{\max} \mathbf{w}_{\max}^* \mathbf{C}}{A_{\max}}. \tag{86}$$

Herewith, we have an alternative for (80) that does not make use of the steering vector $\mathbf{g}_{\max}$, except to define the weight vector $\mathbf{w}_{\max}$. It is noted that $\mathbf{h} = \mathbf{g}_{\max}$ if $\mathbf{C} = A_{\max} \mathbf{g}_{\max} \mathbf{g}_{\max}^*$.

For beamforming without the main diagonal of $\mathbf{C}$ we have

$$\mathbf{w} = \frac{\mathbf{g}}{\left(\sum_{(m,n)\in S}^{N} \left| g_m \right|^2 \left| g_n \right|^2 \right)^{1/2}}. \tag{87}$$

Furthermore, Eq. (84) can be replaced by

$$\mathbf{C}_{\max} = A_{\max} \left(\mathbf{h} \mathbf{h}^* - \mathbf{H} \right), \tag{88}$$

where $\mathbf{H}$ is a matrix of which the diagonal elements are equal to those of $\mathbf{h} \mathbf{h}^*$, and the off-diagonal elements are zero. Eq. (83) is solved when

$$\mathbf{h} = \frac{1}{\left(1 + \mathbf{w}_{\mathbf{max}}^* \mathbf{H} \mathbf{w}_{\mathbf{max}} \right)^{1/2}} \left(\frac{\mathbf{C} \mathbf{w}_{\max}}{A_{\max}} + \mathbf{H} \mathbf{w}_{\max} \right). \tag{89}$$

This is not an explicit expression for $\mathbf{h}$, as $\mathbf{H}$ contains diagonal elements of $\mathbf{h} \mathbf{h}^*$. However, we can work out Eq. (89) iteratively, starting with $\mathbf{h} = \mathbf{g}_{\max}$. Only a few iterations are required for convergence. Now, we do not necessarily have $\mathbf{h} = \mathbf{g}_{\max}$ when $\mathbf{C} = A_{\max} \mathbf{g}_{\max} \mathbf{g}_{\max}^*$.

38

More details about the CLEAN-SC can be found in reference 23.

A successful example of beamforming with CLEAN-SC is shown in Figure 14, which is from airframe noise array measurements on a scale model of the Airbus A340 in the 8×6 m^2 closed test section of the DNW-LLF wind tunnel (see Ref. 23).
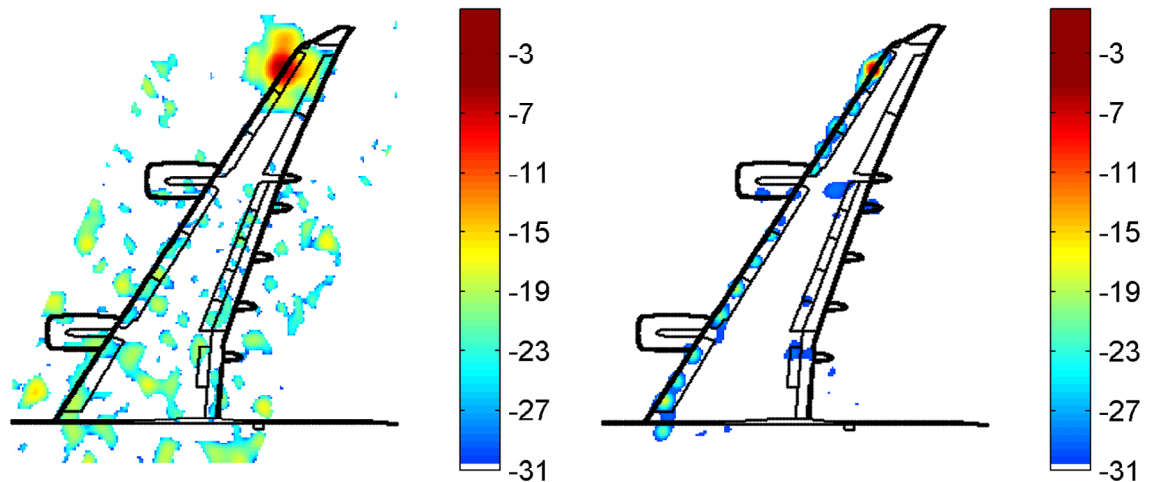

Figure 14 Typical beamforming results from Airbus A340 array measurements in DNW-LLF closed test section; left: Conventional Beamforming, right: CLEAN-SC

5 Moving sources

For array measurements on moving objects, the correct acoustic transfer function from moving source to receiver is required, incorporating the effect of Doppler frequency shift (Refs. 11, 12). For that purpose, an expression has to be used for a moving monopole source in a uniform flow. A brief derivation of such an expression is given below. For a more thorough approach, the reader is referred to reference 44. Using this transfer function, and by proper interpolation of the sampled microphone data, the emitted signals can be reconstructed. This is necessarily a time-domain technique. It will be explained, however, that the signal/noise ratio can be enlarged by a technique, which is similar to the frequency-domain technique of removing the main diagonal (auto-powers) of the cross-power matrix.

5.1 Source description
The acoustic pressure field χ of a monopole source moving in a uniform flow is governed by the differential equation (cf. (27))

$$\nabla^2 \chi - \frac{1}{c^2} \left(\frac{\partial}{\partial t} + \vec{U} \cdot \nabla \right)^2 \chi = \sigma(t) \delta \left(\vec{x} - \vec{\xi}(t) \right), \tag{90}$$

in which $\vec{\xi}(t)$ is the time-dependent source location. Following Dowling and Ffowcs Williams (Ref. 45), equation (90) can be solved by writing the right-hand side as a superposition:

$$\nabla^2 \chi - \frac{1}{c^2} \left(\frac{\partial}{\partial t} + \vec{U} \cdot \nabla \right)^2 \chi = \int_{-\infty}^{\infty} \sigma(\tau) \delta \left(\vec{x} - \vec{\xi}(\tau) \right) \delta(t - \tau) d\tau . \tag{91}$$

Then, the solution can be expressed as

$$\chi(\vec{x}, t) = \int_{-\infty}^{\infty} \sigma(\tau) G \left(\vec{x}, \vec{\xi}(\tau), t, \tau \right) d\tau , \tag{92}$$

where G (the "Green's function") is a solution of

$$\nabla^2 G - \frac{1}{c^2} \left(\frac{\partial}{\partial t} + \vec{U} \cdot \nabla \right)^2 G = \delta \left(\vec{x} - \vec{\xi}(\tau) \right) \delta(t - \tau) . \tag{93}$$

The solution of (93) can be derived from the Green's function of the ordinary wave equation (Ref. 46) by using the following co-ordinate transformation:

$$\begin{cases} t_1 = t, \\ \vec{x}_1 = \vec{x} - \vec{U}t. \end{cases} \tag{94}$$

In the transformed system, we have

$$\nabla_1^2 G - \frac{1}{c^2} \frac{\partial^2 G}{\partial t_1^2} = \delta \left(\vec{x}_1 + \vec{U}t_1 - \vec{\xi}(\tau) \right) \delta(t_1 - \tau) = \delta \left(\vec{x}_1 + \vec{U}\tau - \vec{\xi}(\tau) \right) \delta(t_1 - \tau) . \tag{95}$$

The causal solution of (95) is

$$G = -\frac{\delta \left(t_1 - \tau - \frac{1}{c} \left\| \vec{x}_1 + \vec{U}\tau - \vec{\xi}(\tau) \right\| \right)}{4\pi \left\| \vec{x}_1 + \vec{U}\tau - \vec{\xi}(\tau) \right\|} . \tag{96}$$

Therefore, the causal solution of equation (93), in other words the pressure field induced by an impulsive blow in a uniform flow, is

$$G \left(\vec{x}, \vec{\xi}(\tau), t, \tau \right) = -\frac{\delta \left(t - \tau - \frac{1}{c} \left\| \vec{x} - \vec{\xi}(\tau) - \vec{U}(t - \tau) \right\| \right)}{4\pi \left\| \vec{x} - \vec{\xi}(\tau) - \vec{U}(t - \tau) \right\|} , \tag{97}$$

in which $t > \tau$. It follows that the solution of (91) and hence the solution of (90) is

$$\chi(\vec{x},t) = -\int\limits_{-\infty}^{\infty} \frac{\sigma(\tau)\delta\left(t-\tau-\dfrac{1}{c}\left\|\vec{x}-\vec{\xi}(\tau)-\vec{U}(t-\tau)\right\|\right)}{4\pi\left\|\vec{x}-\vec{\xi}(\tau)-\vec{U}(t-\tau)\right\|}d\tau. \tag{98}$$

To elaborate this integral, introduce the emission time $\tau_e(t)$ as the solution of

$$t-\tau_e = \frac{1}{c}\left\|\vec{x}-\vec{\xi}(\tau_e)-\vec{U}(t-\tau_e)\right\|. \tag{99}$$

As long as the motion is subsonic, this solution is unique. Using (99) and the identity (Ref. 45)

$$\int\limits_{-\infty}^{\infty} f(\tau)\delta\left(\gamma(\tau)\right)d\tau = \sum\frac{f(\tau_0)}{|\gamma'(\tau_0)|}, \text{ where } \gamma(\tau_0)=0, \tag{100}$$

equation (98) can be worked out as

$$\chi(\vec{x},t) = \frac{-\sigma(\tau_e)}{4\pi\left\{c(t-\tau_e)+\dfrac{1}{c}\left(-\vec{\xi}'(\tau_e)+\vec{U}\right)\cdot\left(\vec{x}-\vec{\xi}(\tau_e)-\vec{U}(t-\tau_e)\right)\right\}}. \tag{101}$$

It follows that the transfer function F from moving source in $\vec{\xi}(t)$ to receiver in $\vec{x}$ is given by

$$F\left(\vec{x},\vec{\xi}(\tau_e),t,\tau_e\right) = \frac{\chi(\vec{x},t)}{\sigma(\tau_e)}$$

$$= \frac{-1}{4\pi\left\{c(t-\tau_e)+\dfrac{1}{c}\left(-\vec{\xi}'(\tau_e)+\vec{U}\right)\cdot\left(\vec{x}-\vec{\xi}(\tau_e)-\vec{U}(t-\tau_e)\right)\right\}}, \tag{102}$$

where the relation between t and τ_e is given by equation (99).

It is noted that, in general, an explicit solution for τ_e as a function of t does not exist. In other words, in most cases F is an *implicit* function of t. For source reconstruction, this is not a limitation, because we can solve *explicitly* the inverse problem, i.e., derive from Eq. (99) an explicit expression for t as a function of τ_e. This is worked out in Section 5.2.

5.2 Reconstruction of source signals

Suppose $\chi_n(t)$, $n=1,...,N$ are acoustic pressure signals, recorded by the N microphones. If a monopole source with time-dependent location $\vec{\xi}(t)$ is present, then we can write for the microphone signals

$$\chi_n(t) = F\left(\vec{x}_n,\vec{\xi}(\tau_e),t,\tau_e\right)\sigma(\tau_e)+\varepsilon_n(t), \tag{103}$$

where $\varepsilon_n(t)$ is noise and/or contributions from other sources.

In order to reconstruct the source signal $\sigma(\tau)$ from the microphone signals $\chi_n(t)$, we take in equation (103) a fixed emission time τ_e, independent of microphone number. Then the receiver time t depends on n and it is better to write equation (103) as

$$\chi_n(t_n) = F\left(\vec{x}_n, \vec{\xi}(\tau_e), t_n, \tau_e\right)\sigma(\tau_e) + \varepsilon_n(t_n),\qquad(104)$$

or, briefly,

$$\chi_n(t_n) = F_n(t_n, \tau_e)\sigma(\tau_e) + \varepsilon_n(t_n).\qquad(105)$$

The microphone-dependent receiver times t_n follow from equation (99):

$$t_n - \tau_e = \frac{1}{c}\left\|\vec{x}_n - \vec{\xi}(\tau_e) - \vec{U}(t_n - \tau_e)\right\|.\qquad(106)$$

Though in general an explicit solution τ_e as a function of t_n does not exist, we do have an explicit expression t_n as function of τ_e:

$$t_n = \tau_e + \Delta t_e,\qquad(107)$$

with

$$\Delta t_e = \frac{1}{c\beta^2}\left(-\vec{M}\cdot\left(\vec{x}_n - \vec{\xi}(\tau_e)\right) + \sqrt{\left\{\vec{M}\cdot\left(\vec{x}_n - \vec{\xi}(\tau_e)\right)\right\}^2 + \beta^2\left\|\vec{x}_n - \vec{\xi}(\tau_e)\right\|^2}\right).\qquad(108)$$

A reconstructed source signal $\tilde{\sigma}(\tau_e)$ can be found with the delay-and-sum procedure:

$$\tilde{\sigma}(\tau_e) = \frac{1}{N}\sum_{n=1}^{N}\tilde{\sigma}_n(\tau_e),\qquad(109)$$

with

$$\tilde{\sigma}_n(\tau_e) = \chi_n(t_n)/F_n(t_n, \tau_e).\qquad(110)$$

It is noted that t_n, as calculated by (107), does not coincide with a sample time $k\Delta t$. The best way to proceed is to linearly interpolate the sampled data:

$$\chi_n(t_n) \approx \chi_{n,k}\left((k+1) - \frac{t_n}{\Delta t}\right) + \chi_{n,k+1}\left(\frac{t_n}{\Delta t} - k\right).\qquad(111)$$

To avoid the frequency spectrum from being spoiled by side lobes from higher frequencies, the sample frequency should be taken higher than two times the maximum analysis frequency, without raising the low pass filter cut-off frequency. This problem was addressed for instance by Howell et al (Ref. 12).

5.3 Reconstruction of source auto-powers

5.3.1 Straightforward method

A straightforward way to calculate the frequency spectrum of a source signal is to evaluate equation (109) for $\tau_e = k\Delta t,\ k = 1,...,K$ and then perform an FFT, resulting in pressure amplitudes

$$a(\tilde{\sigma}) = \frac{1}{N}\sum_{n=1}^{N} a(\tilde{\sigma}_n) . \tag{112}$$

The source auto-power estimate $\tilde{A}$ is calculated as

$$\tilde{A} = \frac{1}{2}\left|a(\tilde{\sigma})\right|^2 = \frac{1}{2N^2}\left|\sum_{n=1}^{N} a(\tilde{\sigma}_n)\right|^2 = \frac{1}{2N^2}\sum_{m=1}^{N}\sum_{n=1}^{N} a(\tilde{\sigma}_m)a(\tilde{\sigma}_n)^* . \tag{113}$$

5.3.2 Error estimate

With equations (105), (110), and (113), we can write

$$\tilde{A} = \frac{1}{2}\left|a(\sigma) + \frac{1}{N}\sum_{n=1}^{N} a\left(\varepsilon_n/F_n\right)\right|^2 . \tag{114}$$

Now assume that $\varepsilon_n(t)$ is stochastic and incoherent from one microphone to the other (e.g. wind noise). Then, after averaging, the following expression remains:

$$\tilde{A} = \frac{1}{2}\left|a(\sigma)\right|^2 + \frac{1}{2N^2}\sum_{n=1}^{N}\left|a\left(\varepsilon_n/F_n\right)\right|^2 = A + \frac{1}{2N^2}\sum_{n=1}^{N}\left|a\left(\varepsilon_n/F_n\right)\right|^2 . \tag{115}$$

5.3.3 Removal of auto-powers

Consider the following approximation of equation (113):

$$\tilde{A} = \frac{1}{2N(N-1)}\sum_{\substack{m=1 \\ n\neq m}}^{N}\sum_{n=1}^{N} a(\tilde{\sigma}_m)a(\tilde{\sigma}_n)^* = \frac{1}{2N(N-1)}\left(\left|\sum_{n=1}^{N} a(\tilde{\sigma}_n)\right|^2 - \sum_{n=1}^{N}\left|a(\tilde{\sigma}_n)\right|^2\right). \tag{116}$$

Again under the assumption that $\varepsilon_n(t)$ is stochastic and incoherent, and after averaging over many time periods, we simply get $\tilde{A} = A$. In other words, the expected error is now zero now.

This method is analogous to the elimination of the main diagonal from the cross-power matrix (Section 4.2). Just like its frequency-domain counterpart, the right-hand side of equation (116) may become negative, which is not physical. This may happen, for instance, if a secondary source exists, giving a coherent contribution to $\varepsilon_n(t)$, or in case of insufficient averaging.

5.4   Microphone weights

It is possible to apply microphone weights v_n (see Section 4.1) in the processing techniques of this chapter. Equations (113) and (116) are then changed into

$$\tilde{A} = \frac{1}{2} \sum_{m=1}^{N} \sum_{n=1}^{N} v_m v_n a(\tilde{\sigma}_m) a(\tilde{\sigma}_n)^* \bigg/ \sum_{m=1}^{N} \sum_{n=1}^{N} v_m v_n \qquad (117)$$

and

$$\tilde{A} = \frac{1}{2} \sum_{m=1}^{N} \sum_{\substack{n=1 \\ n \neq m}}^{N} v_m v_n a(\tilde{\sigma}_m) a(\tilde{\sigma}_n)^* \bigg/ \sum_{m=1}^{N} \sum_{\substack{n=1 \\ n \neq m}}^{N} v_m v_n \, . \qquad (118)$$

5.5   Applications

As examples of applications of the beamforming technique with moving sources, results are given of array measurements on a wind turbine model in the DNW-LLF (Refs. 13, 47), and on landing aircraft at Schiphol airport (Refs. 10, 23). Typical source plots are shown in Figure 15 and Figure 16, respectively.
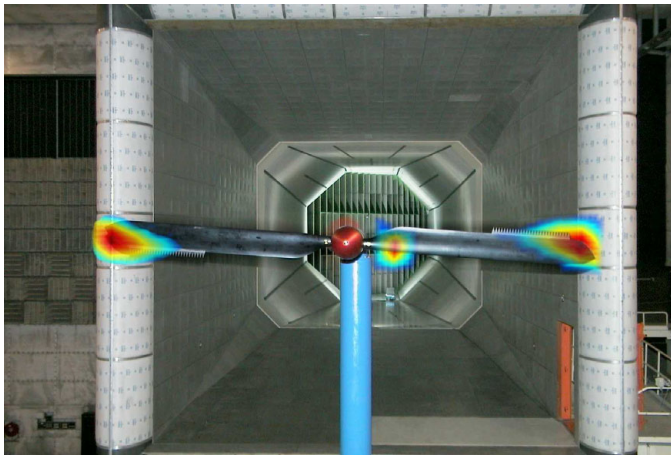

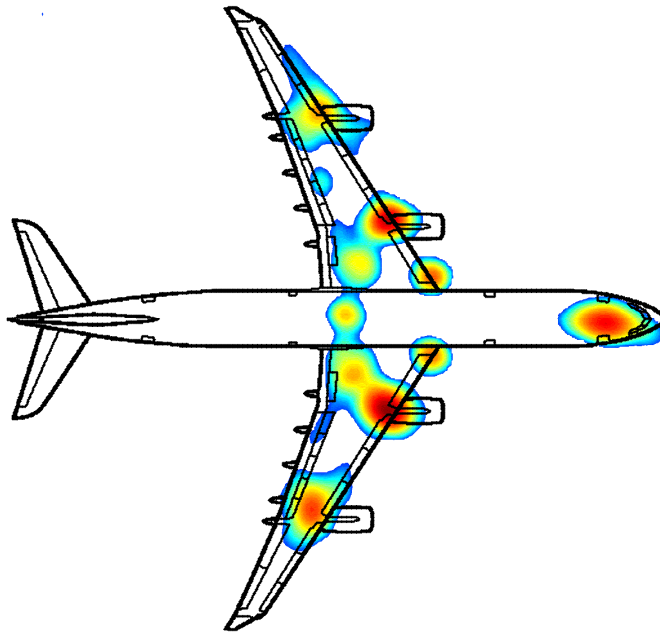*Figure 15   Wind turbine rotor in DNW-LLF*

Figure 16 Airbus A340 during approach

6 Conclusion

Microphone arrays are convenient tools for locating aero-acoustic sources on wind tunnel models and on flying aircraft. In this paper, an introduction is given on the beamforming techniques that can be applied for that purpose.

References

1. Grosche, F.-R., Stiewitt, H., and Binder, B., "Acoustic wind-tunnel measurements with a highly directional microphone ", *AIAA Journal* Vol. 15., No. 11, pp. 1590-1596, 1977.
2. Schlinker, R.H., "Airfoil trailing edge noise measurements with a directional microphone", AIAA Paper 77-1269. 1977.
3. Fisher, M.J., and Harper Bourne, M., "Source location in jet flows", Aeronautical Research Council Report ARC 35/383/N910, 1974.
4. Billingsley, J., and Kinns, R., "The acoustic telescope", Journal of Sound and Vibration, Vol. 48, No. 4, pp. 485-510, 1976.
5. Holthusen, H.H., and Smit, H., "A new data acquisition system for microphone array measurements in wind tunnels", AIAA Paper 2001-2169, 2001.

6. Takano, Y., Horihata, K., Kaneko, R., Matsui, Y., and Fujita, H., "Analysis of sound source characteristics of Shinkansen cars by means of X-shaped microphone array", Internoise 96, Liverpool, 1996.

7. Barsikow, B., "Experiences with various configurations of microphone arrays used to locate sound sources on railway trains operated by the DB AG", *Journal of Sound and Vibration*, Vol. 193, No. 1, 1996, pp. 283-293.

8. Michel, U., Barsikow, B., Helbig, J., Hellmig, M., and Schüttpelz, M., "Flyover noise measurements on landing aircraft with a microphone array", AIAA Paper 98-2336, 1998.

9. Piet, J.-F., and Elias, G., "Localization of acoustic source from a landing aircraft with a microphone array", AIAA Paper 99-1811, 1999.

10. Sijtsma, P., and Wal, H.M.M. van der, "Identification of noise sources on civil aircraft in approach using a phased array of microphones", NATO symposium SET-079 "Capabilities of Acoustics in Air-Ground and Maritime Reconnaissance, Target Classification and - Identification", Lerici, Italy, 26-28 April 2004, NLR-TP-2004-166, 2004.

11. Barsikow, B., and King III, W.F., "On removing the Doppler frequency shift from array measurements of railway noise", *Journal of Sound and Vibration*, Vol. 120, No. 1, 1988, pp. 190-196.

12. Howell, G.P., Bradley, A.J., McCormick, M.A., and Brown, J.D., "De-Dopplerization and acoustic imaging of aircraft fly-over noise measurements", *Journal of Sound and Vibration*, Vol. 105, No. 1, 1986, pp. 151-167.

13. Sijtsma, P., Oerlemans S., and Holthusen, H.H., "Location of rotating sources by phased array measurements", AIAA Paper 2001-2167, NLR-TP-2001-135, 2001.

14. Johnson, D.H., and Dudgeon, D.E., *Array Signal Processing*, Prentice Hall, 1993.

15. Dougherty, R.P., "Turbulent decorrelation of aeroacoustic phased arrays: Lessons from atmospheric science and astronomy", AIAA Paper 2003-3200, 2003.

16. Brooks, T.F., and Humphreys Jr., W.M., "Effect of directional array size on the measurement of airframe noise components", AIAA Paper 99-1958, 1999.

17. Sijtsma, P., and Holthusen, H.H., "Source location by phased measurements in closed wind tunnel test sections", AIAA Paper 99-1814, NLR-TP-99108, 1999.

18. Guidati, S., Brauer, C., and Wagner, S., "The Reflection Canceller – Phased array measurements in a reverberating environment", AIAA Paper 2002-2462, 2002.

19. Sijtsma, P., and Holthusen, H.H., "Corrections for mirror sources in phased array processing techniques", AIAA Paper 2003-3196, NLR-TP-2003-123, 2003.

20. Blacodon, D., and Elias, G., "Level estimation of extended acoustic sources using a parametric method", *Journal of Aircraft*, Vol. 41, No. 6, 2004, pp. 1360-1369.

21. Brooks, T.F., and Humphreys, W.M., "A deconvolution approach for the mapping of acoustic sources (DAMAS) determined from phased microphone arrays", *Journal of Sound and Vibration*, Vol. 294, 2006, pp. 856-879.

22. Ravetta, P., Burdisso, R., and Ng, W., "Noise source localization and optimization of phased array results (LORE)", AIAA Paper 2006-2713, 2006.

23. Sijtsma, P., CLEAN based on spatial source coherence, *International Journal of Aeroacoustics*, Vol. 6, No. 4, 2007, pp. 357-374, NLR-TP-2007-345, 2007.

24. Sijtsma, P., and Stoker, R.W., "Determination of absolute contributions of aircraft noise components using fly-over array measurements", AIAA Paper 2004-2960, NLR-TP-2004-167, 2004.

25. Böhning, P., and Siller, H.A., "Study of a de-convolution method for aircraft flyover measurements", AIAA Paper 2007-3474, 2007.

26. Press, W.H., Teukolski, S.A., Vetterling, W.T., and Flannery, B.P., *Numerical Recipes*, Cambridge, 1994.

27. Lynn, P.A., and Fuerst, W., *Introductory Digital Signal Processing with Computer Applications*, Wiley, 1998.

28. Lighthill, M.J., *Introduction to Fourier Analysis and Generalised Functions*, Cambridge, 1978.

29. Harris, F.J., "On the use of windows for harmonic analysis with the discrete Fourier transform", *Proceedings of the IEEE*, Vol. 66, No. 1, 1978, pp. 51-83.

30. Liu, Y., Quayle, A.R., Dowling, A.P., and Sijtsma, P., "Beamforming correction for dipole measurement using 2-D microphone arrays", *Journal of the Acoustical Society of America*, Vol. 124, No.1, 2008, pp. 182-191.

31. Amiet, R.K., "Refraction of sound by a shear layer", *Journal of Sound and Vibration*, Vol. 58, No. 2, 1978, pp. 467-482.

32. Schulten, J.B.H.M., "Computation of aircraft noise propagation through the atmospheric boundary layer", *Proceedings of the 5th International Congress on Sound and Vibration*, Adelaide, Australia, NLR-TP-97374, 1997.

33. Mueller, T.J. (Ed.), *Aeroacoustic Measurements*, Springer, 2002.

34. Underbrink, J.R., and Dougherty, R.P., "Array design of non-intrusive measurement of noise sources", Noise-Con 96, Seattle, Washington, 29 September-2 October 1996.

35. Sijtsma, P., "Optimum arrangements in a planar microphone array", Presented at the First CEAS-ASC Workshop: "Wind Tunnel Testing in Aeroacoustics", DNW, 5/6 November 1997.

36. Abramowitz, M., and Stegun, I.A. (Eds.), *Handbook of Mathematical Functions*, Dover Publ., 1970.

37. Daigle, G.A., Piercy, J.E., and Embleton, T.F.W., "Line-of-sight propagation through atmospheric turbulence near the ground", *Journal of the Acoustical Society of America*, Vol. 74, No. 5, 1983, pp. 1505-1513.

38. Tatarski, V.I., "The effects of the turbulent atmosphere on wave propagation", *Israel Program for Scientific Translations*, Jerusalem, 1971.

39. Tatarski, V.I., *Wave Propagation in a Turbulent Medium*, McGraw-Hill, 1961.

40. Wal, H.M.M. van der, and Sijtsma, P., "Flap noise measurements in a closed wind tunnel with a phased array", AIAA Paper 2001-2170, NLR-TP-2001-632, 2001.

41. Dougherty, R.P., "Source location with sparse acoustic arrays; interference cancellation", Presented at the First CEAS-ASC Workshop: Wind Tunnel Testing in Aeroacoustics, DNW, 5/6 November 1997.

42. Sarradj, E., "A fast signal subspace approach for the determination of absolute levels from phased microphone array measurements", Journal of Sound and Vibration, Vol. 329, No. 9, 2010, pp. 1553-1569.

43. Högbom, J.A., "Aperture synthesis with a non-regular distribution of interferometer baselines", *Astron. Astrophys. Suppl.*, No. 15, 1974, pp. 417-426.

44. Howe, M.S., *Acoustics of Fluid-Structure Interactions*, Cambridge University Press, 1998.

45. Dowling, A.P., and Ffowcs Williams, J.E., *Sound and Sources of Sound*, Wiley, 1983.

46. Treves, F., *Basic Partial Differential Equations*, Academic Press, 1975.

47. Oerlemans, S., Schepers, J.G., Guidati, G., and Wagner, S., "Experimental demonstration of wind turbine noise reduction through optimized airfoil shape and serrations", *Proceedings of the European Wind Energy Conference and Exhibition*, Copenhagen, 2-6 July 2001, NLR-TP-2001-324, 2001.